Multiphoton ionization dynamics of barium Rydberg states in intense femtosecond pulses

D. A. Tate
Department of Physics and Astronomy, Colby College, Waterville, Maine 04901

T. F. Gallagher
Department of Physics, University of Virginia, Charlottesville, Virginia 22901

(Received 9 February 1998)

We have investigated multiphoton ionization of Ba $6snl$ Rydberg states by intense 200-fs laser pulses. Specifically, we have excited Ba atoms to the $6sns$ and $6snd$ $15<n<\infty$ states using two nanosecond lasers. The atoms were then irradiated with the fs pulses produced by a mode-locked, regeneratively amplified Ti:sapphire laser that is stepwise-tunable between 790 and 850 nm. We have used both the fundamental light and the second harmonic (395–425 nm) to investigate the ionization dynamics in these two wavelength regions. In contrast to previous experiments, in which laser pulses 5 ps or longer were used, our results indicate that excitation of Ba^+ Rydberg states and Ba^{2+} photoions is relatively insensitive to the femtosecond laser wavelength. In addition, we find that, as the Kepler orbital period of the Ba Rydberg electron becomes comparable to this very small laser pulse width, the inner electron ionization process no longer appears to be instantaneous to the outer electron, and the outer electron is not projected onto Ba^+ Rydberg states. [S1050-2947(98)03110-2]

PACS number(s): 32.80.Rm, 31.50.+w

I. INTRODUCTION

The photoionization dynamics of Rydberg states of two-electron atoms when irradiated by intense picosecond or femtosecond laser pulses is a topic of significant interest largely because it is possible to drive transitions of the ionic core while the outer Rydberg electron is almost unaffected [1–5]. One of the more striking phenomena is the process of inner electron ionization, observed by Stapelfeldt *et al.* [6] and Jones and Bucksbaum [7]. In both cases the authors observed that if excited bound Ba Rydberg states were exposed to an intense laser pulse of duration short compared to the classical orbital period of the Rydberg electron that multiphoton ionization of the ionic core occurred while the Rydberg electron remained bound. Jones and Bucksbaum exposed bound $6snk$ Stark states in an electric field $E=1/3n^5$ to 70-ps pulses of 355-nm light. In a classical view of the Stark states the orbital angular momentum l oscillates between 0 and n with a period $T_S=2\pi n^4$ when the field is $E=1/3n^5$. When l is small the Rydberg electron comes near the ionic core and can interact with the $6s$ electron or absorb a visible photon. For $n>26$, T_S exceeds the laser pulse duration and multiphoton ionization of the inner electron was observed while the outer electron remained bound, forming Ba^+ Rydberg states.

Stapelfeldt *et al.* exposed the zero-field Ba $6sns$ and $6snd$ states to 5-ps pulses of a dye laser at 620 nm, a wavelength matching the three-photon Ba^+ $6s\rightarrow 7p$ transition. Classically, a ns or nd electron returns to the core in the Kepler time $T_K=2\pi n_I^3$, where n_I is the effective quantum number of the $6sns$ or $6snd$ state and is given by $n_I=\sqrt{-2W}$, where W is the energy of the $6sns$ or $6snd$ state. Consequently, multiphoton ionization of the inner $6s$ electron without removal of the outer electron should occur for values of $n_I\geqslant 32$, for which the Kepler time exceeds the laser pulse duration. In fact, it was observed to occur for $n_I\geqslant 35$, in reasonable agreement with expectation.

In both experiments, starting from a single bound Rydberg state leads to a range of Ba^+ Rydberg states that is approximately consistent with projecting the bound Rydberg state wave function onto Ba^+ wave functions, as would occur if the inner electron were removed instantaneously from the atom. If the initial bound state has an effective principal quantum number n_I, the maximum value of the effective quantum number n_{II} of the Ba^+ Rydberg states resulting from such a projection is expected to be $n_{II}\approx\sqrt{2}n_I$. In practice the values observed by Stapelfeldt *et al.* and Jones and Bucksbaum were $n_{II}/n_I=1.32$ and $\sqrt{2}$, respectively.

The experiments reported here were begun with the goal of learning more about why inner electron ionization ceases to occur as n is decreased. We have used substantially shorter pulses than used before, as short as 200 fs. With the 200-fs pulse we expected to see inner electron ionization from initial Ba Rydberg states of n_I as low as 11, a value much lower than those observed in the previous experiments, but it is only observed for n_I as low as 14. Inner electron ionization fails to occur when the outer electron is removed along with or instead of the inner electron. Initially we had expected inner electron ionization to fail either because the outer electron was directly photoionized by the laser or because a doubly excited resonance was excited, which decayed by autoionization. In fact, the results of the experiments described here suggest that at low n failure occurs because the departure of the inner electron is not instantaneous and that the departing inner electron knocks the outer electron out of the atom. In the sections that follow we describe the experimental approach, the results, and the conclusions we draw from them.

II. EXPERIMENTAL APPROACH

The basic experimental apparatus is shown in Fig. 1. Two 5-ns pulses from dye lasers are used to excite Ba ground-

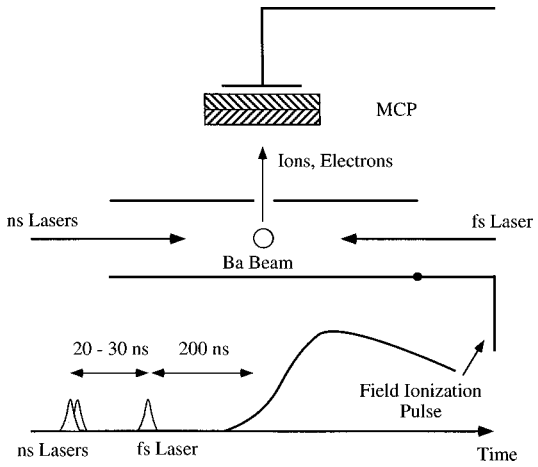

FIG. 1. Diagram of interaction region between Ba atoms in an atomic beam and lasers. Initially, Ba atoms initially in the ground state are excited to $6sns$ and $6snd$ states by two nanosecond laser pulses. Some 20–30 ns later, the femtosecond laser ionizes the Ba atoms. A large field-ionization pulse then pushes Ba^+ and Ba^{2+} photoions toward a microchannel plate detector, and also field ionizes Ba and Ba^+ Rydberg states.

state atoms in an effusive atomic beam to the $6sns$ and $6snd$ states. The first laser is tuned to excite the $6s^2\ ^1S_0 \rightarrow 6s6p\ ^1P_1$ resonance transition at 554 nm, and the second laser is tunable between 432 and 417 nm, enabling us to drive the $6s6p\ ^1P_1 \rightarrow 6sns\ ^{1,3}S$ and $6s6p\ ^1P_1 \rightarrow 6snd\ ^{1,3}D$ transitions where $15<n<\infty$. Both lasers are weakly focused using a 500-mm focal length lens, and the laser fluence is sufficient to significantly deplete the ground-state atom population in the interaction region.

Approximately 30 ns after the nanosecond lasers have excited the Ba atoms to a Rydberg state, the atoms are irradiated with 200-fs pulses derived from an amplified mode-locked Ti:sapphire oscillator. The femtosecond pulses propagate at 180° to the nanosecond pulses, and both are perpendicular to the atomic beam. The excitation takes place between a pair of capacitor plates separated by 3 mm. Using this device, we can either field ionize Rydberg states of Ba and Ba^+ using a 50-kV/cm, 500-ns rise-time electric field pulse, or gently push the Ba^+ and Ba^{2+} photoions out of the interaction region towards a dual microchannel plate detector (MCP) with a 100-V pulse. The field ionization pulse rises quickly enough to ionize Ba^+ Rydberg ions before expelling them from between the field plates. In both cases the ions leave the interaction region via a 50-μm-wide, 3-mm-long slit aligned along the laser beam propagation direction and travel through an 8-cm-long field free region to the MCP. The 30-ns delay between the ns and the fs laser pulses ensures that the Ba atoms with which the short-pulse laser interacts are all in either the ground state or the Rydberg state of interest. The femtosecond laser is stepwise tunable between 790 and 850 nm, and we can frequency double the light in a 0.5-mm-long BBO crystal to produce pulses between 395 and 425 nm. The pulses obtained from the fs laser have a maximum energy of 2 mJ for the fundamental and 250 μJ in the second harmonic. The ion time-of-flight signal from the MCP is displayed on a digitizing oscilloscope, and selected time bins of the digitized signal can be gated and averaged using a computer to observe the behavior of the Ba and Ba^+ field-ion and Ba^+ and Ba^{2+} photoion yields as the second ns dye laser is tuned over the Ba Rydberg states.

III. EXPERIMENTAL RESULTS

We discuss our data in the following three sections. When we use the field-ionization pulse the signals due to photoionization and field ionization of Ba and Ba^+ Rydberg states are resolved in time. To provide some feeling for the signals, we first show the time-resolved signals obtained using the fundamental and second harmonic of the femtosecond laser. We then present the spectra obtained by setting the detection gate on specific parts of the time-resolved signal, typically the Ba^+ Rydberg signal, and scanning the nanosecond laser over the Rydberg states. Finally, we describe the data obtained from observing the Ba^+ and Ba^{2+} photoion signal as the nanosecond laser was tuned over the Ba $6snl$ Rydberg series.

A. Field ionization time-of-flight signals

An example of a time-of-flight spectrum of species arising when a field ionization pulse is applied to the atoms and ions after the interaction of the Ba Rydberg states with the femtosecond laser can be seen in Fig. 2. This spectrum was obtained with the fundamental of the Ti:sapphire laser at 830 nm, with the Ba atoms initially in the $6s24d$ state. Figure 2(a) shows the field-ionization signal when the femtosecond laser is blocked, i.e., the entire signal arises from the field ionization of the $6s24d\ ^1D$ state created by the dye lasers. Figure 2(b) shows the Ba^+ and Ba^{2+} photoions created by just the femtosecond laser from the Ba $6s^2$ ground state when the dye lasers are blocked. There are several interesting features to this spectrum. First, the Ba^{2+} yield is comparable to that of Ba^+, in direct contrast to the situation of Refs. [6] and [7] where Ba^{2+} production was insignificant unless the laser was tuned to a multiphoton resonance in Ba^+ (Ref. [6]), or unless the Nd:YAG third harmonic was used (Ref. [7]). Second, the generation of Ba^{2+} photoions in the most intense part of the laser focus leads to a clearly observable depletion in the center of the Ba^+ signal. Finally, there is also direct excitation of Ba^+ Rydberg states by just the femtosecond laser at this wavelength, which appears in the spectrum as the feature labeled ''*A*.'' This observation is somewhat surprising, given that the two routes for formation of Ba^+ Rydberg states are either the direct 10-photon process from the $6s^2$ ground state of Ba, or the 7-photon process from either the $6s$ or $5d$ states of Ba^+. (Ten photons above the Ba $6s^2$ state is 2200 cm^{-1} below the Ba^{2+} limit, while 7 photons above the Ba^+ $6s$ and $5d$ states is respectively 8000 and 2700 cm^{-1} below the same limit, at zero laser intensity.) Most likely the Ba^+ Rydberg states are brought into resonance by ac Stark shifts during the pulse, as observed previously [8–11]. The ac stark shifts are quite large. Under the conditions of this experiment the ponderomotive shift at the peak intensity is 6 eV (48 000 cm^{-1}), and we estimate that the low-lying levels of Ba^+ shift by about 1 eV (8000 cm^{-1}). Together these shifts can easily bring the Rydberg states into resonance during the laser pulse.

Figure 2(c) shows the time-of-flight spectrum which results when the 830-nm femtosecond pulses irradiate the Ba

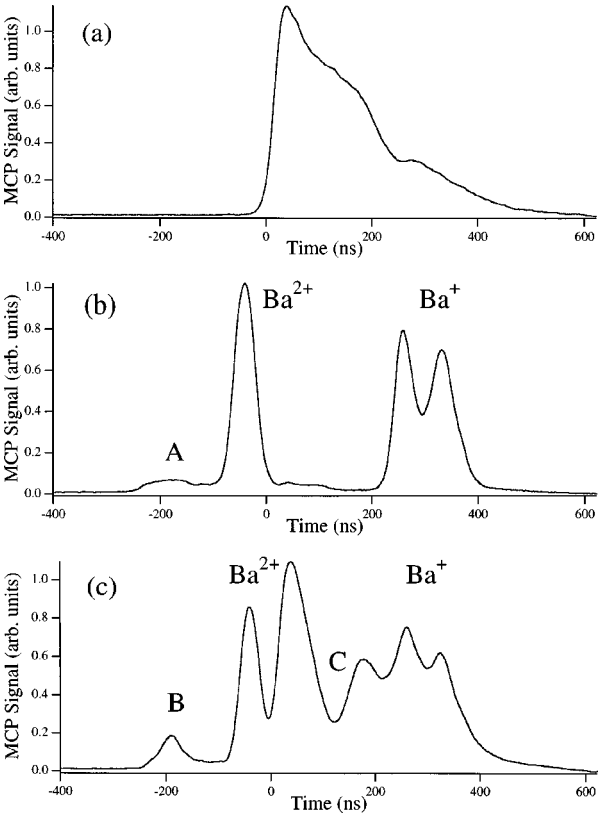

FIG. 2. Time-of-flight Ba ion spectra obtained using the 830-nm fundamental of the Ti:sapphire laser. (a) shows the field-ionization spectrum of the Ba $6s24d$ state when there is no femtosecond laser light. In (b), the Ba^+ and Ba^{2+} ion signals resulting from photoionization of the Ba $6s^2$ ground state by 830-nm light from the femtosecond laser is shown. Note the creation of Ba^+ Rydberg states directly by just the femtosecond laser (labeled ''*A*''). In (c) the ion spectra taken with the fundamental of the femtosecond laser at 830 nm when the $6s24d$ state is initially excited by the nanosecond lasers. Inner electron ionization is evident from the enhancement of the Ba^+ Rydberg state field-ionization signal (labeled ''*B*'') and the decrease of the Ba^+ photoion signal. Also evident is a ''hole'' in the Ba field-ionization signal (labeled ''*C*'') due to inner electron photoionization converting Ba Rydberg states into Ba^+ Rydberg states.

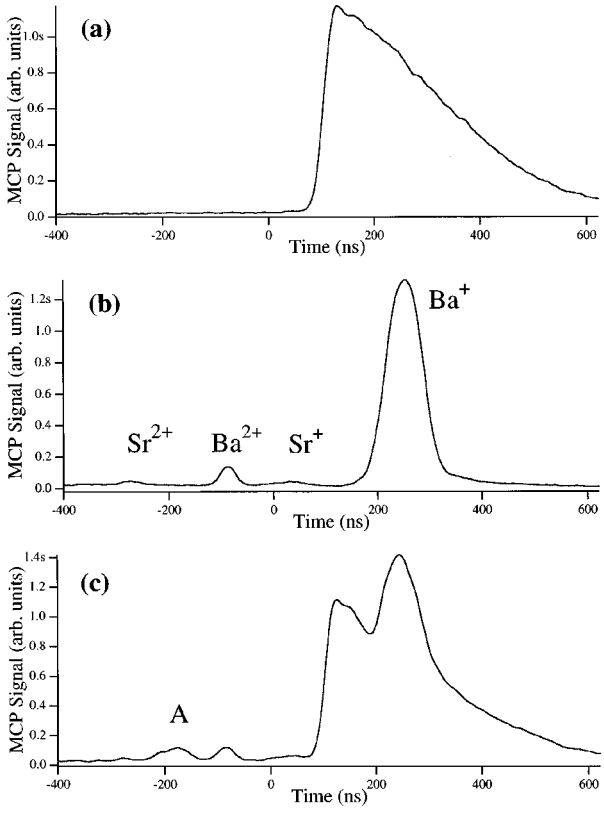

FIG. 3. Time-of-flight Ba ion spectra obtained using the 415-nm second harmonic of the Ti:sapphire laser. (a) shows the field-ionization spectrum of the Ba $6s31d$ state when there is no femtosecond laser light. In (b), the Ba^+ and Ba^{2+} ion signals resulting from photoionization of the Ba $6s^2$ ground state by 415-nm second harmonic is shown. Note the creation of Sr^+ and Sr^{2+} from strontium contamination of the Ba in the oven. In (c) the ion spectra taken with the second harmonic of the femtosecond laser at 415 nm when the $6s31d$ state is initially excited by the nanosecond lasers. Inner electron ionization is evident from appearance of the Ba^+ Rydberg state field-ionization signal (labeled ''*A*'').

$6s24d\ ^1D$ Rydberg state. The most significant feature in the spectrum is the enhancement of the Ba^+ Rydberg state signal (labeled ''*B*''), and a corresponding reduction in the Ba^{2+} photoionization signal, a clear signature of inner-electron ionization. Related to this effect is the decrease in the Ba^+ photoion signal, a consequence of ''shelving'' population in the Ba Rydberg states, which are less easily ionized than the ground state. Finally, the removal of population from the Ba Rydberg states to the Ba^+ Rydberg states is evident as a dip, labeled ''*C*,'' in the Ba field ionization spectrum immediately after its rising edge. In Fig. 2(a), the falloff of the Ba field ion signal is relatively slow, whereas in Fig. 2(c), there is a hole immediately after the field ion signal maximum, followed by a rise again immediately before the Ba^+ photoion signal.

The creation of Ba^+ Rydberg states from Ba Rydberg states by the femtosecond laser is very different from the behavior observed in previous experiments [6,7]. In the previous works, no Ba^+ Rydberg state excitation was observed unless the short-pulse laser was tuned to a multiphoton resonance in Ba^+ [6], or the photon energy was sufficient to ensure that the excitation pathway did not contain transitions through the spectral region containing a high density of short-lived Ba autoionizing states (i.e., a single photon of the short-pulse laser had to reach approximately 30 000 cm^{-1} above the Ba^+ $6s$ state) [7].

When we used the second harmonic of the femtosecond laser we obtained time-of-flight signals that were slightly different from the ones shown in Fig. 2. An example, obtained by populating the Ba $6s31d\ ^1D_2$ Rydberg state and exposing the atoms to a 415-nm femtosecond pulse and a 29-kV/cm field pulse, is shown in Fig. 3. Figure 3(a) shows the field-ionization signal from just the Ba Rydberg $6s31d\ ^1D$ state, obtained when the femtosecond laser is blocked. In Fig. 3(b), the photoion signal from just the femtosecond laser is shown. The other experimental parameters (Ba oven temperature, MCP voltage) are the same as in Fig. 2. As can be seen, the Ba^{2+} yield is much lower, by a factor of 30, than the Ba^+ yield, which is itself comparable to the Ba^+ yield when the 830-nm fundamental light is used. Also visible in the signal are Sr^+ and Sr^{2+} photoions that are present due to the small strontium contamination in the

barium sample in our oven. Since no evidence of the strontium ions can be seen in Fig. 2(b), it is clear that Sr^+ and Sr^{2+} ions are much more efficiently generated by the blue light than by the infrared light. This contrasts with barium, where the singly charged and doubly charged ion yields are greater with the infrared light. Given that Sr and Sr^+ both have resonance lines near 415 nm while Ba and Ba^+ do not, this contrast is hardly a surprise.

When the Ba $6snl$ states are irradiated with the 415-nm light from the femtosecond laser, Ba^+ $n'l'$ states are excited, with a corresponding reduction in the Ba^{2+} signal. There is one clear difference that is apparent when the data in Figs. 2(c) and 3(c) are compared, which is that the Ba^+ $n'l'$ and Ba^{2+} signal amplitudes are comparable in Fig. 3(c), whereas the Ba^+ Rydberg state signal is only some 20% of the Ba^{2+} photoion signal in Fig. 2(c). Presumably the 830-nm light excites the inner electron through regions where it is much more efficiently coupled to the outer electron than when 415-nm light is used, resulting in the formation of short-lived autoionizing states that decay to low-lying Ba^+ states, which then photoionize.

Although the Ba and Ba^+ resonance lines are not near 400 nm, there are transitions between excited states of Ba and Ba^+ that suggest the possibility of resonances near 400 nm. Consequently, we carried out a preliminary survey of the excitation efficiency for creating Ba^{2+} photoions from Ba^+ ions in the $6s$ state at various wavelengths between 395 and 425 nm. The Ba^+ ground-state ions were generated using the nanosecond lasers, with the second laser tuned to 417 nm, just above the threshold for photoionization of the Ba $6s6p\ ^1P_1$ state. Since the Ti:sapphire laser is not continuously tunable, we stepped the laser wavelength in 5-nm steps from 790 to 850 nm, each time reoptimizing the modelocked laser, the grating stretcher and compressor system, and the BBO frequency doubling crystal. However, the resulting photoion spectrum showed no resonant structure. We also measured the relative yield for production of Ba^+ and Ba^{2+} photoions starting in the Ba $6s^2$ ground state as a function of the wavelength of the femtosecond laser for wavelengths between 395 and 425 nm, and found that the maximum yield of Ba^{2+} was approximately 30% of the Ba^+ photoion yield at the same wavelength.

B. The field-ionization spectrum

It is instructive to observe the field ionization signal from Rydberg states of Ba^+, as a function of the wavelength of the nanosecond laser driving the Ba $6s6p\ ^1P_1 \rightarrow 6snl$ transition. An example of such a scan is shown in Fig. 4, which was obtained using the 830-nm light from the femtosecond laser (the 415-nm data were essentially identical). The region of excitation of the initial Ba Rydberg states is from 41 700 to 42 020 cm^{-1}, or from just below the $6s21d\ ^3D$ state almost up to the ionization limit. To obtain the data shown in Fig. 4, several gates were placed on the time-of-flight signal. Figure 4(a) is the signal from a gate placed over the Ba field ionization signal and the Ba^+ photoion signal, while Fig. 4(b) is the signal from a gate placed over the Ba^{2+} photoion signal. Figures 4(c) through 4(f) are from gates placed at successively earlier times just before the Ba^{2+} photoion signal so as to capture the signals from Ba^+ Rydberg states.

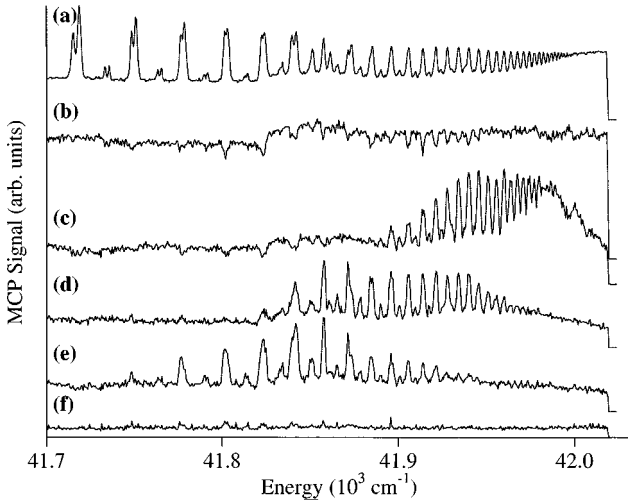

FIG. 4. Ba^+ and Ba^{2+} photoion, and Ba and Ba^+ Rydberg state field ion signals, as a function of the initial Ba $6snl$ state. The femtosecond laser wavelength was 830 nm, and the amplitude of the field-ionization pulse was 44.5 kV/cm. The energy range of the initial Ba Rydberg states excited is from 41 700 to 42 020 cm^{-1}, i.e., from just below $6s21d$ up to the ionization limit. (a) through (f) correspond to progressively earlier time gates: (a) is the Ba^+ photoion and Ba $6snl$ field-ionization signal (250-ns-wide gate); (b) is the Ba^{2+} photoion signal (40-ns gate); (c) through (f) are Ba^+ $n'l'$ field-ionization signals (25-ns gates), each successive gate being set earlier than the previous one. Clearly, the gate in (f) is set too early to catch any of the Ba^+ $n'l'$ signal, but in (e) through (c), the Ba^+ field ionization signal arrives progressively later as the n of the initial Ba $6snl$ state is increased. In (b), the depletion of the Ba^{2+} photoion signal when the nanosecond lasers are resonant with a Ba Rydberg state can be seen. The depletion disappears at high n since the gate also captures the high-n' Ba^+ field-ionization signal.

Each of the four gates in Figs. 4(c) through 4(f) was 25 ns wide, whereas the gate in Fig. 4(b) was 40 ns wide, and that in Fig. 4(a) was 250 ns wide. Apparently, the gate in Fig. 4(f) was at too early a time to catch a significant amount of the Ba^+ field ionization signal, but in Fig. 4(e), a field ion signal from Ba^+ states generated when the femtosecond laser irradiates the Ba $6s23d$ states and higher $6sns$ and $6snd$ states is quite apparent. No signal is visible from Ba^+ Rydberg states resulting from irradiation of Ba $6s22d$ and lower states either because no Ba^+ $n'l'$ states are produced, or those that are are too tightly bound to the Ba^{2+} core to be field ionized in the 44.5-kV/cm pulse we applied. The lack of a Ba^+ Rydberg signal for low n states is surprising since the previous results suggest that it should be visible down to approximately the $6s14d$ state (i.e., when $n_1=11$, since the quantum defect of the $6snd$ states is ≈ 2.7).

As the nanosecond laser is tuned to higher Ba $6snl$ states, the Ba^+ field ionization signal moves to later times, as evidenced by its disappearance from the gate in Fig. 4(e), and its successive appearance and disappearance from the gates in Figs. 4(d) and 4(c). Finally, for very high Ba $6snl$ states, the resulting Ba^+ field-ionization signal becomes indistinguishable from the Ba^{2+} photoion signal, resulting in the gradual decline in signal from the high frequency end of Fig. 4(c). (The high Ba^+ $n'l'$ states ionize early in the pulse, and so observe a temporal field variation that is almost identical to that of the Ba^{2+} photoions. The low Ba^+ $n'l'$ states ionize

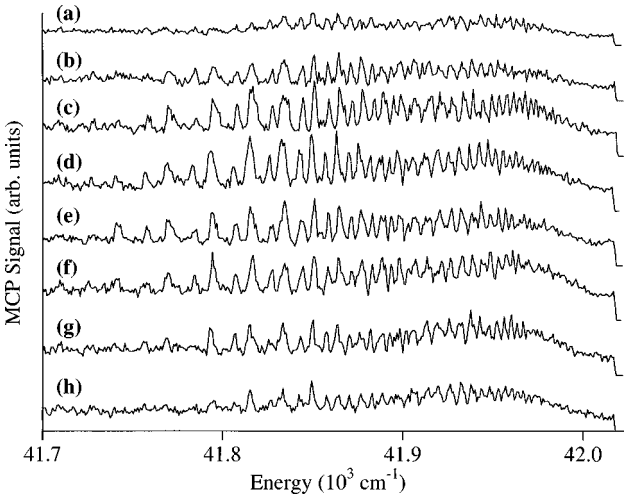

FIG. 5. Variation $Ba^+ n'l'$ field-ionization signal arising from different initial Ba $6snl$ states with the length of the femtosecond laser pulse. The femtosecond laser wavelength was 830 nm, and the amplitude of the field-ionization pulse was 44 kV/cm. The range of initial Ba $6snl$ states was the same as shown in Fig. 4. The pulse length was changed by changing the length of the compression arm of the chirped-pulse amplification system. In (a) through (d) the pulse lengths were 1.7, 1.1, 0.5, and 0.35 ps (±20%) respectively, and the laser chirp was positive, and in Fig. 6(e), the pulse length was 0.2 ps (±20%, no chirp). In (f) through (h) the pulse lengths were 0.35, 0.65, and 0.95 ps (±20%) respectively, and the laser chirp was negative.

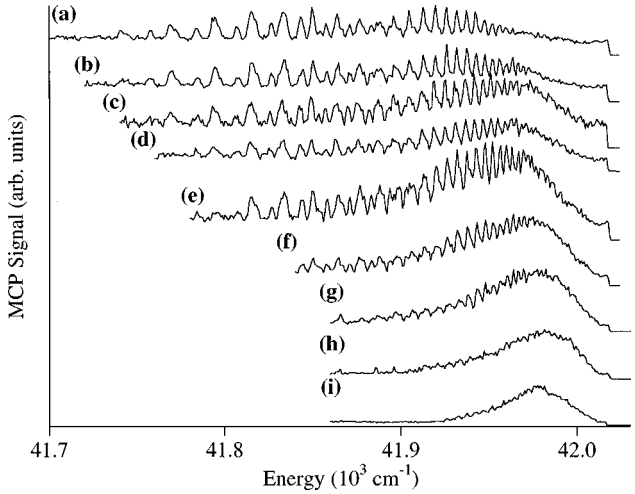

FIG. 6. Variation Ba^+ $n'l'$ field-ionization signal arising from different initial Ba $6snl$ states with the amplitude of the field-ionization pulse. The femtosecond laser wavelength was 830 nm. The amplitudes of the field-ionization pulses used in each scan (together with the corresponding maximum effective principal quantum number, n_{II}, of Ba^+ Rydberg states which arises from a given Ba Rydberg state) are as follows: (a) 44.4 kV/cm ($n_{II}=15.5$); (b) 37.6 kV/cm ($n_{II}=16.2$); (c) 32.5 kV/cm ($n_{II}=16.8$); (d) 24.6 kV/cm ($n_{II}=17.9$); (e) 19.5 kV/cm ($n_{II}=19.1$); (f) 11.6 kV/cm ($n_{II}=21.7$); (g) 5.1 kV/cm ($n_{II}=26.6$); (h) 2.5 kV/cm ($n_{II}=31.8$); (i) 1.2 kV/cm ($n_{II}=38.3$); the n_{II} values are determined from the amplitude of the field-ionization pulse E by $E=1/(2n_{II}^4)$.

later, and consequently the resulting Ba^{2+} ions gain a larger impulse from the electric field than the Ba^{2+} photoions, and so arrive at the detector at an earlier time.) Another feature visible in Fig. 4(b) is the depletion of the Ba^{2+} photoion signal when the nanosecond laser is tuned to a Ba Rydberg state. This phenomenon is discussed more fully in the next section.

The principal conclusion of the two previous works on this subject [6,7] was that the Rydberg states of Ba^+ are formed when the Kepler, or Stark, period of the Ba $6snl$ Rydberg electron is longer than the laser pulse being used to photoionize it. On the other hand, when the period is shorter that the laser pulse, the Rydberg electron in Ba ionizes, followed by the inner $6s$ electron, resulting in Ba^{2+}. In both Refs. [6] and [7], however, this conclusion was arrived at by changing the Kepler period (by exciting different $6snl$ states) from shorter than to longer than the fixed laser pulse length and observing the onset of the Ba^+ Rydberg signal. A more direct test is to change the pulse length of the laser and see if the onset of Ba^+ Rydberg state production follows the pulse length in the expected way.

It is relatively easy to increase the length of the laser pulse by detuning the delay in the grating compressor after the regenerative amplifier, which enabled us to stretch the pulse from its minimum value of 200 fs to as much as 1.7 ps. (Due to the reduced peak power the doubling efficiency was substantially reduced, which prevented us from obtaining data with the second harmonic of the Ti:sapphire laser.) When the delay in the compressor is detuned from the value necessary to give the optimum output pulse length, the resulting pulse has either positive or negative chirp. Hence, we obtained data with the delay either shorter or longer than its optimum value to see if the chirp had any effect on the data. These data are shown in Fig. 5. The pulse widths in scans (a) through (h) are 1.7, 1.1, 0.5, 0.35, 0.2, 0.35, 0.65, and 0.95 ps, respectively. The pulse widths are estimated from the laser bandwidth and the settings of the grating expander and compressor; and have an estimated uncertainty of ±20%. In traces (a) through (d), the pulse has positive chirp, and in (f) through (h), it has negative chirp. As can be seen, the positive and negative chirps lead to similar results. In traces (a) and (h), where the pulse length is 1.7 and 0.95 ps, respectively, the lowest Ba $6snl$ state that gives rise to an identifiable Ba^+ field ionization signal is $6s24d$, in which the Rydberg electron has a Kepler period of 1.5 ps. Trace (b), taken with a 1.1-ps pulse also shows a Ba^+ signal arising from the Ba $6s23d$ state, where the Kepler period is 1.3 ps. Hence, the data in traces (a), (b), and (h), taken with long pulses, seem to confirm the hypothesis advanced in Refs. [6] and [7], i.e., Ba^+ Rydberg states are observed if the Kepler period is longer than the laser pulse duration. On the other hand, the data in traces (c) through (g), taken with shorter pulses, seem to contradict the hypothesis. In these traces, the pulse length was between 0.2 and 0.65 ps. However, the lowest Ba state that contributes to the Ba^+ field-ionization signal is the $6s22d$ state, which has a Kepler period of 1.1 ps, far longer than the duration of the laser pulse.

Further insight can be obtained by using different amplitudes of field-ionization pulse to detect the Ba^+ Rydberg ions. In Fig. 6 we show the Ba^+ Rydberg signal, obtained with several amplitudes of pulse, as the ns laser exciting the bound Rydberg states is scanned. In all cases the femtosecond laser wavelength was 830 nm and the pulse length was 200 fs. It is not unexpected that as the ionizing pulse ampli-

TABLE I. Experimental determination of the effective quantum number for the initial Ba Rydberg state (n_I) and the highest final Ba^+ Rydberg state which is formed by inner-electron photoionization (n_{II}).

Ba state	n_I	n_{II}	n_{II}/n_I
$6s34d$	31.3	38.3	1.22
$6s31d$	28.3	31.8	1.12
$6s29d$	26.3	26.6	1.01
$6s27d$	24.3	21.7	0.88
$6s25d$	22.3	19.1	0.86
$6s24d$	21.3	17.9	0.84
$6s23d$	20.3	16.8	0.83
$6s22d$	19.3	15.5	0.80

tude is reduced the lowest bound Rydberg state leading to a signal increases, and it is useful to represent these results quantitatively. Each field-ionization pulse amplitude implies the lowest Ba^+ effective quantum number that can be ionized. Thus if no Ba^+ Rydberg signal is observed we know that any Ba^+ Rydberg states produced have a lower effective quantum number than $n_{II}=1/(2E)^{1/4}$, where E is the amplitude of the ionizing field pulse. The bound Rydberg state at which the Ba^+ Rydberg signal disappears defines n_I, and the values of n_I and n_{II} and the ratio n_{II}/n_I are given in Table I. Note that for higher n states $n_{II}/n_I=1.22$, in reasonable agreement with the values obtained in the earlier experiments. However, as the principal quantum number of the initial Rydberg state is reduced the ratio falls to 0.80, indicating qualitatively different behavior.

C. Photoion Spectra

The data described above clearly show that Rydberg states of Ba^+ are created from Rydberg states of Ba by inner-electron photoionization by the femtosecond laser, in the limit where the Kepler period of the outer electron is much greater than the laser pulse width. As the Kepler period is reduced to the laser pulse duration of 200 fs, we expected to see Ba^+ Rydberg states for initial Ba $6snd$ Rydberg states of n_I as low as 11. However, we only see Ba^+ Rydberg signals for n_I as low as 19. It is also clear from Table I that as the principal quantum number of the initial Rydberg state is decreased toward $n=20$ that the resulting Ba^+ Rydberg states are, increasingly, more tightly bound than expected, raising the possibility that the Ba^+ Rydberg states are created, but in lower-lying states than expected, so that we are unable to detect them by field ionization. Accordingly, we have used an alternative method, observing the depletion of the Ba^{2+} photoionization signal as the ns laser producing the bound Rydberg states is scanned. Specifically, we observed the behavior of both the Ba^+ and Ba^{2+} photoionization signals as the wavelength of the second nanosecond laser was scanned over the Ba Rydberg series.

The principle of this approach is easily understood by considering the effect of the femtosecond laser on the Ba^+ and Ba^{2+} signals as the wavelength of the second nanosecond laser is scanned over the bound Rydberg states. For high n, the valence electron is far from the ionic core and photoionization of the Ba $6snl$ states by the femtosecond laser is less likely than multiphoton ionization of the Ba $6s^2$ ground state. Consequently, when the nanosecond dye lasers are tuned to a Rydberg state, there is a dip, or depletion, in the Ba^+ signal since a significant fraction of the Ba atoms are in a Rydberg state, which has a lower probability of ionizing than the atoms left in the ground state. On the other hand, as n is decreased the single photon ionization rate of the Rydberg state becomes larger than the multiphoton ionization rate of the ground-state atoms, the dips in the Ba^+ signal start to fill in, and eventually, for sufficiently low n, become peaks in the photoion signal. In the case of the Ba^{2+} photoion signal, and for sufficiently high n, the femtosecond laser ionizes the inner electron, leaving a Ba^+ ion in a Rydberg state. Since this species also has a low photoionization cross section, creation of this species manifests itself by a depletion of the Ba^{2+} photoion signal. When the dye lasers are tuned to excite a low-lying Rydberg state, in which the outer electron ionizes when irradiated by the femtosecond laser, no depletion is apparent in the Ba^{2+} signal. The dips in the Ba^{2+} photoion signal are therefore a good signature of when the inner electron of the Ba $6snl$ state is ionizing in preference to the outer electron. When only the femtosecond laser is used the Ba^{2+} signal originates from multiphoton ionization of Ba^+, which is produced on the rising edge of the femtosecond pulse. If the Ba atoms are first excited to a higher Rydberg state the multiphoton ionization of the inner electron is unchanged. If the outer electron remains on the atom, the result is a Ba^+ Rydberg state and a decrease in the Ba^{2+} signal. Consequently, even if we are unable to detect the resulting Ba^+ Rydberg state by field ionization, we are able to detect the production of Ba^+ Rydberg states by observing the decrease in the Ba^{2+} signal.

In these experiments, only a small field is required to push the ions out of the interaction region toward the MCP. We used either a 400-V/cm pulse from an SCR circuit, or a 300 V/cm pulse from a Hewlett-Packard pulse generator, which field ionized Ba $6snl$ states with $n \geqslant 30$. Care had to be taken to ensure that there was no significant ionization of the Rydberg states by the nanosecond lasers, especially in the case of the data taken with the second harmonic of the Ti:sapphire laser, where it is possible for the fluence of the light from the nanosecond dye laser to be comparable to that of the femtosecond light at 415 nm. This problem becomes progressively worse at lower n, and we took care to attenuate the nanosecond lasers until we could identify no photoionization, which we could attribute to the nanosecond lasers.

Examples of the Ba^+ and Ba^{2+} photoion spectra as a function of the energy of the initial Ba $6snl$ state are shown in Figs. 7 and 8. Figure 7 shows the Ba^+ and Ba^{2+} photoion spectra when the Ti:sapphire fundamental at 830 nm is used to photoionize the barium atoms, and Fig. 8 shows the corresponding spectra when the 415-nm light is used. In each figure, the upper trace (a) is the Ba^+ spectrum, while the lower trace (b) is the Ba^{2+} spectrum. The energy range of the $6snl$ states excited by the nanosecond lasers shown in Figs. 7 and 8 is from 41 260 cm^{-1} to 42 020 cm^{-1}, corresponding to a range from just below the $6s15d\ ^1D$ and $6s15d\ ^3D$ states, to just below the Ba ionization limit. In the Ba^+ spectrum shown in Fig. 7(a), the dips that occur when the outer electron is shelved in a Rydberg state are clearly visible at high n, but as n is reduced they slowly decrease in depth and

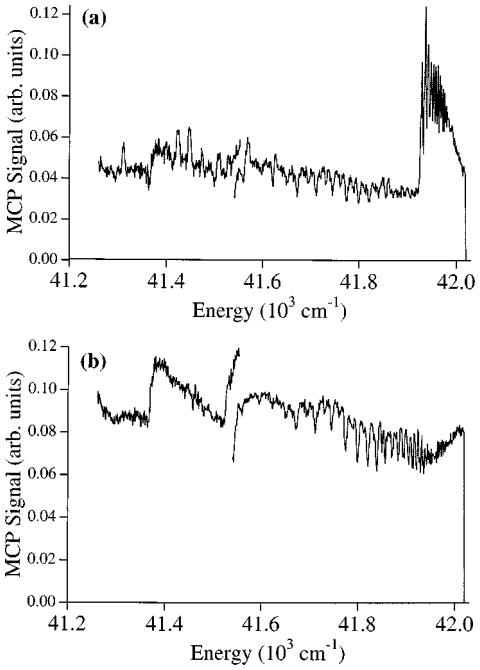

FIG. 7. Variation of (a) Ba^+ and (b) Ba^{2+} photoion yields with the energy of the initial Ba $6snl$ state for the fundamental of the Ti:sapphire laser system (830 nm). The energy range of the initial Ba Rydberg states excited is from 41 560 cm^{-1} to 42 020 cm^{-1}, i.e., from just below $6s15d$ up to the ionization limit. Breaks in the data are due to each of these figures being comprised of data from different laser scans. Steps visible in (a) and (b) near 41 600 and 41 750 cm^{-1} are due to oven variations. The sudden rise in the Ba^+ signal near 42 000 cm^{-1} is caused by the onset of Ba Rydberg state field ionization in the 300-V/cm pulse used to push the photoions toward the MCP.

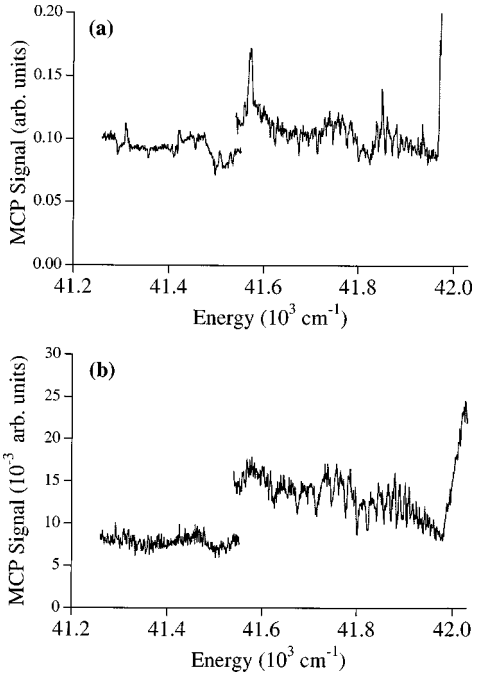

FIG. 8. Variation of (a) Ba^+ and (b) Ba^{2+} photoion yields with the energy of the initial Ba $6snl$ state for the second harmonic of the Ti:sapphire laser system (415 nm). The energy range of the initial Ba Rydberg states excited is from 41 560 to 42 020 cm^{-1}, i.e., from just below $6s15d$ up to the ionization limit. Breaks in the data are due to each of these figures being comprised of data from different laser scans. The sudden rise in the Ba^+ and Ba^{2+} signals near 42 000 cm^{-1} is caused by the onset of Ba and Ba^+ Rydberg state field ionization in the 300-V/cm pulse used to push the photoions toward the MCP.

become peaks at low n. In Fig. 7(b), the Ba^{2+} spectrum is shown; at the positions that correspond to the dips in the Ba^+ spectrum in Fig. 7(a), dips also appear in the Ba^{2+} spectrum, but where there are peaks in the Ba^+ spectrum, the Ba^{2+} spectrum is flat and featureless. (The changes in the background levels of the Ba^+ and Ba^{2+} signals are due to oven temperature changes.) The point at which the dips become peaks in the Ba^+ spectrum, and the dips disappear in the Ba^{2+} spectrum appears to be around the $6s17d\ ^1D$ state, corresponding to an effective quantum number of the outer electron of $n_I \approx 14$. This value of n_I is substantially lower than the value obtained from the field-ionization spectra of Fig. 4, $n_I = 19$. Apparently inner-electron ionization and Ba^+ Rydberg states production occurs, for n_I as low as 14, but the resulting Ba^+ Rydberg states are more tightly bound than expected, since the 50-kV/cm pulse can ionize Ba^+ Rydberg states of $n_{II} = 15$. However, we note that, even with this detection technique we do not see inner electron ionization as low as $n_I = 11$, the $6s14d$ state as expected on the basis of the Kepler orbit time.

Also apparent in Figs. 7(a) and 7(b) [and in Figs. 8(a) and 8(b)] is an increase in both the Ba^+ and Ba^{2+} signals above approximately the $6s35l$ states, which is due to (respectively) field ionization of the Ba and Ba^+ Rydberg state in the ≈400-V/cm pulse we used to push out the ions toward the MCP detector. Since the pulse had a slightly different amplitude in Figs. 7 and 8, the actual $6snl$ state that starts to field ionize is different in each figure, being slightly higher in Fig. 8. In addition, it can also be seen that the field-ionization signal of the Ba^+ Rydberg states turns on much more slowly than that of the Ba Rydberg states. This effect is much more evident in Fig. 8(b) than in Fig. 7(b), since the ratio of Ba^+ Rydberg states to Ba^{2+} photoions is higher when the 415-nm light is used, as can be seen by comparing Figs. 2(c) and 3(c). The slower turn-on of the field-ionization signal from the Ba^+ Rydberg states arises from the fact that the projection of the initial Ba Rydberg state onto the Ba^+ Rydberg state leads to a range of Ba^+ Rydberg states when the inner electron is photoionized.

Behavior similar to that of Fig. 7 is apparent in the 415-nm data, shown in Figs. 8(a) and 8(b). Clearly, in Fig. 8(b), the dips in the Ba^{2+} spectrum disappear around the $6s18d\ ^1D$ state, corresponding to $n_I \approx 15$. As in Fig. 7(b) this spectrum shows evidence for inner electron ionization for lower n_I than the field-ionization spectra of Fig. 4, but not as low a value of n_I as expected from a comparison of the laser pulse width to the Kepler orbit time. The better signal-to-noise ratio of the Ba^+ spectrum of Fig. 8(a), as compared to Fig. 7(a), shows a more complex and rather interesting behavior. The peaks start appearing for the $6snd\ ^1D$ states below $n = 18$; however, there are also peaks near the $6s26d\ ^3D_2$ state and at the $6s37d$ state. On the other hand, dips in the Ba^+ photoion spectrum are still visible for the $6snd\ ^3D$ states at the lowest n investigated, namely, $n = 15$, and also for the $6sns$ states as low as $6s17s$.

Quite possibly the marked difference between the singlet and triplet *nd* states derives from the fact that the autoionizing $6p_{3/2}nd$ states accessible from the $6snd\ ^1D_2$ using 415-nm light are wider than those accessible from the $6snd\ ^3D_2$ states at the same wavelength [12]. Off-resonant excitation at 415 nm would be more likely to cause autoionization of the singlet $6snd$ states than the triplet $6snd$ states. The $6s15d\ ^3D$ state has an effective quantum number of $n_I \approx 12$ for the outer electron, while for the $6s17s$ state it is $n_I \approx 13$. The Kepler orbital periods for these values of n_I are 262 and 333 fs, respectively, and the pulsewidth of our laser was approximately 200 fs. The peaks in the Ba^+ spectrum near the $6s27d\ ^3D_2$ and $6s37d$ states occur because these states have a significant component of different terms of the $5d7d$ configuration in their wave functions. The $6s27d\ ^3D_2$ state is approximately 25% $5d7d\ ^1D_2$ in character, while the $6snd$ states near $n=35$ have a significant percentage of $5d7d\ ^3P$ character [13]. These states photoionize (or autoionize) since the $5d7d$ wave function is localized much closer to the nucleus than the Rydberg electron wave function in a $6snl$ state. On the other hand, there is a distinct behavior for the lower $6snl$ states. Peaks corresponding to the photoionization of the $6snd\ ^1D$ states can be seen in the Ba^+ spectrum for $n \leqslant 18$ ($n_I \leqslant 15$), whereas dips corresponding to the $6snd\ ^3D$ and $6sns$ states are clearly apparent down to the lowest states investigated, $n=15$ ($n_I=12$) for the $6snd\ ^3D$ states, and $n=17$ ($n_I=13$) for the $6sns$ states. Clearly, the photoionization of the $6snd\ ^3D$ and $6sns$ states is in agreement with the expected behavior when one compares the Kepler periods of these states with the pulse length of the femtosecond laser. However, the $6snd\ ^1D$ states seem to ionize even when their Kepler periods are over twice as long as the pulse length.

IV. DISCUSSION

As we have already noted, with a 200-fs laser pulse we would expect to see inner electron ionization for n_I as low as 11, whereas we actually observe $n_I=12$ for the $6snd\ ^3D$ states, and $n_I=13$ for the $6sns$ states, giving reasonable agreement between experiment and theory. On the other hand, there is significant disagreement between theory and experiment for the $6snd\ ^1D$ states. This deviation from our expectation can be understood in the following way. For an intense short laser pulse the probability of the Rydberg *ns* or *nd* electrons being ionized by the laser pulse is unity if the electron comes within some small volume, $\sim 50a_0^3$ at the ionic core. Thus for a pulse duration T_L the probability of ionization P_{ion}, of a Rydberg electron is given by the fraction of the Kepler orbit time T_K represented by the laser pulse duration T_L. Thus for $T_K \geqslant T_L$

$$P_{\text{ion}}=\frac{T_L}{T_K}. \tag{1}$$

The laser pulse duration T_L corresponds to the Kepler orbit time for a value of the effective quantum number n_L defined by $T_L=2\pi n_L^3$, so we can rewrite P_{ion} for a state with effective quantum number $n_I > n_L$ as

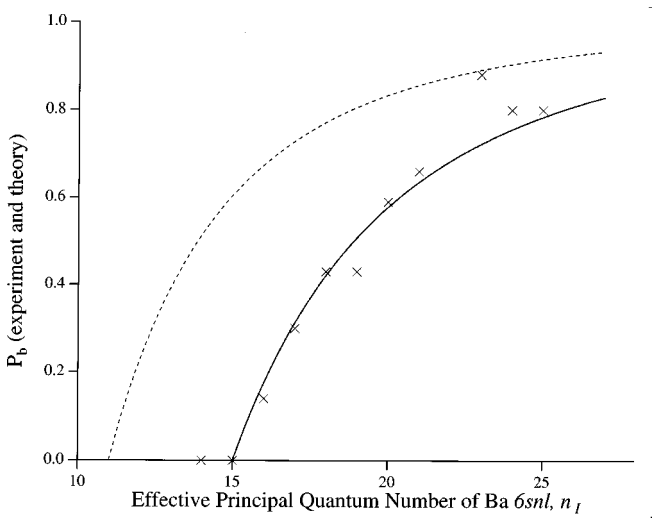

FIG. 9. Plots of the experimental and theoretical values of P_b, the probability of the Ba $6snl$ Rydberg electron remaining bound as a function of the Rydberg electron's effective principal quantum number, n_I. The experimental data points, labeled (×), are for the $6snd\ ^1D$ states, and are obtained from the Ba^{2+} photoionization depletion data shown in Fig. 7(b). The estimated uncertainty in the values of P_b is ±10%. Also shown are the values of P_b calculated from the equation $P_b=1-(n_L/n_I)^3$, for two cases: $n_L=11$, corresponding to $T_L=200$ fs (– – –), and $n_L=15$, corresponding to $T_L=500$ fs (——).

$$P_{\text{ion}}=\left(\frac{n_L}{n_I}\right)^3. \tag{2}$$

The probability of the electron's remaining bound is, of course,

$$P_b=1-\left(\frac{n_L}{n_I}\right)^3. \tag{3}$$

The probability of multiphoton ionization of the inner electron should be independent of the state of the outer electron, and we therefore expect the fraction of bound $6snd$ Rydberg atoms which undergoes inner electron ionization to be proportional to P_b.

The best measure of inner electron ionization of the $6snd\ ^1D$ states is the decrease in the Ba^{2+} signal, and to obtain a fractional yield P_b for each bound state we divide the depth of the dip in the Ba^{2+} signal of Fig. 8, the 415-nm data, by the amplitude of the Ba field-ionization signal of Fig. 4(a), a measure of the initial population in the Ba $6snd$ states. (The much poorer signal-to-noise ratio of the $6snd\ ^3D$ and $6sns$ dips precluded our being able to analyze these states by the same method.) The resulting yields are then multiplied by a normalization factor, which gives a yield of 0.8 at $n_I=25$, and the resulting normalized yields are plotted in Fig. 9. Also plotted in Fig. 9 are graphs of P_b using two values of n_L, 11 and 15, corresponding to laser pulse durations of 200 and 500 fs. The data match the calculated curve for a 500-fs pulse, but not the 200-fs pulse. This discrepancy is presumably a manifestation of the nonresonant transition from the $6snd\ ^1D$ states to the rapidly autoionizing $6p_{3/2}nd$ states at 415 nm.

A second clear difference between these experiments and the previous experiments occurs in the apparent distribution of final Ba^+ Rydberg states. We use the word apparent to reflect the fact that deriving an n distribution requires an assumption about how field-ionization occurs. In the previous experiments the authors assumed that the Ba^+ Rydberg states ionized classically in the field ionization pulse, at the field $E=1/(2n_{II}^4)$. With this assumption they concluded that the initial state of effective quantum number n_I led to values of n_{II} consistent with the projection of the neutral Ba Rydberg state onto the Ba^+ Rydberg states. The approximate range was $n_I<n_{II}<\sqrt{2}n_I$. The highest values of n_{II} were $1.32n_I$ [6] and $1.4n_I$ [7]. Using the same assumption of classical field ionization to analyze our data we find the values of Table I. At higher $n_{II}=1.22n_I$, close to the value reported in the previous work. However, as n is decreased we find n_{II} decreases to $0.80n_I$. It appears that as n is decreased progressively more of the high n_{II} part of the expected distribution is missing. Since the yield curves of Fig. 9 suggest that there is the expected abrupt change in the yield at $n_I \approx n_L$, most likely the final state distribution is not the one expected for a projection, shown in Fig. 10(a) but more like the distribution shown in Fig. 10(b), i.e., the final-state distribution is more heavily weighted at lower n_{II}, which have smaller orbital radii. Since Table I contains values of $n_{II}/n_I<1$ it is worth bearing in mind that we have assumed field ionization to occur at $E=1/(2n_{II}^4)$. In fact, if Ba^+ Rydberg states of $m>4$ are made the ionization will occur at fields in excess of $E=1/2n_{II}^4$ and the n_{II} values of Table I are too low.

The important point is that as the initial state is decreased from $n_I=32$ to $n_I=22$ the final-state distribution changes dramatically. A projection corresponding to the instantaneous removal of the inner electron does not happen. What we see is a reflection of the interaction between the two electrons in the finite time it takes the inner electron to escape from the atom. That the removal of the electron appears instantaneous when the outer electron is in a high n but not a low n state is not so surprising when one considers that the natural atomic time for the outer electron is the Kepler time T_K, which is shorter for low n than for high n. Eichmann *et al.* have studied inner-shell electron ionization starting from high-l Sr $5d_{5/2}nl$ states, and they have observed results similar to ours, i.e., that the outer electron is not simply projected onto the Sr^+ Rydberg states. They have, in addition, done classical calculations of the energy exchange between the two electrons during the ejection of the inner electron, and the results are consistent with both sets of experimental results and our comments above [14].

V. CONCLUSIONS

We have investigated multiphoton ionization of Ba $6sns$ and $6snd$ Rydberg states by intense 200-fs laser pulses using both infrared (830 nm) and blue (415 nm) wavelengths. Specifically, we investigated the evolution of the photoionization process from inner electron ionization to Rydberg electron ionization as a function of the effective principal quantum number of the Ba $6snl$ state, n_I, and as a function of the laser pulse length, T_L. In contrast to previous experiments, in which ps laser pulses were used, our results indicate that excitation of Ba^+ Rydberg states and Ba^{2+} photoions is relatively insensitive to the femtosecond laser wavelength [6,7]. Our results also imply that inner electron ionization gives way to Rydberg electron ionization at a higher n_I than one would expect from a comparison of the classical Kepler period, T_K, with T_L, at least for $6snd\ ^1D$ states, though this conclusion is less clear for $6snd\ ^3D$ states. In addition, we find that, as the Kepler orbital period of the Ba Rydberg electron becomes comparable to this very small laser pulsewidth, the inner electron ionization process no longer appears to be instantaneous to the outer electron, and the outer electron is not projected onto Ba^+ Rydberg states of effective principal quantum number n_{II} where $n_I<n_{II}<\sqrt{2}n_I$, but rather onto a narrower range of $n_{II}\approx n_I$.

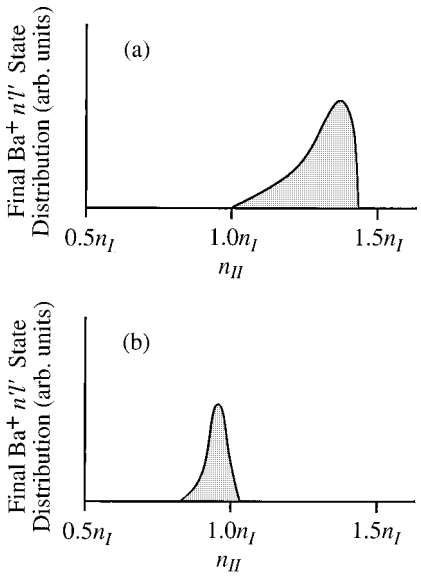

FIG. 10. Final Ba^+ Rydberg state distributions when the Ba $6s$ electron is photoionized by the femtosecond laser for different initial values of the effective principal quantum number of the Ba $6snl$ state, n_I. (a) shows the final-state distribution for $n_I>30$, as reported in Refs. [6] and [7], and in general agreement with the data shown in Fig. 6(i). (b) shows the final-state distribution for $n_I \leqslant 25$, as inferred from the data in Figs. 6(a) through 6(d).

ACKNOWLEDGMENTS

We would like to thank R. R. Jones for many discussions during the course of this work. It is a pleasure to acknowledge useful discussions with W. Sandner and U. Eichmann regarding this problem. We are also grateful to D. W. Schumacher for the data acquisition software used in these experiments. Funding for these experiments has been provided by the U.S. DOE, Office of Basic Energy Sciences.

[1] F. Robischeaux, Phys. Rev. A **47**, 1391 (1993).
[2] N. J. van Druten and H. G. Muller, Phys. Rev. A **52**, 3047 (1995).
[3] R. Grobe and J. H. Eberly, Phys. Rev. A **48**, 623 (1993).
[4] B. Walker, M. Kaluza, B. Sheehy, P. Agostini, and L. F. DiMarco, Phys. Rev. Lett. **75**, 633 (1995).
[5] L. G. Hanson, J. Zhang, and P. Lambropoulos, Phys. Rev. A **55**, 2232 (1997).
[6] H. Stapelfeldt, D. G. Papaiouannou, L. D. Noordam, and T. F. Gallagher, Phys. Rev. Lett. **67**, 3223 (1991).
[7] R. R. Jones and P. H. Bucksbaum, Phys. Rev. Lett. **67**, 3215 (1991).
[8] R. R. Freeman, P. H. Bucksbaum, H. Milchberg, S. Darack, D. Schumacher, and M. E. Geusic, Phys. Rev. Lett. **59**, 1092 (1987).
[9] M. P. de Boer and H. G. Muller, Phys. Rev. Lett. **68**, 2747 (1992).
[10] J. G. Story, D. I. Duncan, and T. F. Gallagher, Phys. Rev. Lett. **70**, 3012 (1993).
[11] R. B. Vrijen, J. H. Hoogeneraad, H. G. Muller, and L. D. Noordam, Phys. Rev. Lett. **70**, 3016 (1993).
[12] O. C. Mullins, Y. Zhu, E. Y. Xu, and T. F. Gallagher, Phys. Rev. A **32**, 2234 (1985).
[13] M. Aymar and P. Camus, Phys. Rev. A **28**, 850 (1983).
[14] U. Eichmann, M. Seng, C. Rosen, and W. Sandner (unpublished).